Chapter 1
Introduction

Traditionally, matter is classified into three categories: gaseous, liquid, and solid. This classification applies to simple materials with isotropic characteristics. Their properties can be predicted with conventional models and do not depend on the direction they are measured, as well as any transport phenomena that occurs within the domain. Anisotropic materials behave differently, often non-linearly, and their ample range of application created the need for detailed theories to explain the causes and consequences of materials with internal microstructure. Even more so, theory has enabled the design of materials by predicting transitions and specific morphologies.

The discovery of an intermediate state of matter was made by Friedrich Reinitzer in 1888 [1] and Otto Lehmann in 1889 [2], who observed a double melting point for a substance related to cholesterol. This fourth state of matter resulted in a mesomorphous state and the term liquid crystal (LC) was coined as it features crystal-like ordering and liquid-like fluidity. The set of properties exhibited by liquid crystals consists of a unique combination of optical, electromagnetic and rheological behavior that makes them of particular interest for the design of smart and functional materials. Since the 1960s the LC field has burgeoned and conquered diverse fields that range from mathematics to biosciences. After the success of basic and applied research in display technology, the strategies for modern LC research are guided by the work of Pierre–Gilles de Gennes [3–6]., who envisioned the utility of LC in bioenginering applications.

All liquid crystal-based technologies rely on the atypical elastic and optical properties which project molecular events up to the visible range in a fast and accurate manner. To highlight some applications, the easy orientability of LC molecules is convenient for the development

of new semiconductor devices [7–9], photonics and lasing [10–12], improvement of energy conversion [13, 14], low-voltage electro-optic devices [15–18], actuators [19, 20], nematic colloids and metamaterials [21–26], and biodetection [27–35]. An approach to a biosensor using planar geometries was first presented [27], where the assembly of proteins in the interface caused the formation of patterns in the LC phase. In 2009 a sensor functionalized for viruses and bacteria was possible using a monodisperse emulsion of LC micro–droplets with a high sensitivity, obtaining fast determining optical changes under low concentration of external agents [32]. Regarding bacterial contamination, a LC–based biosensor was developed where micrometer droplets interacted with endotoxins [34]. More recently, the detection of specific types of peptides allows for the screening of amyloid fibril formation in biomedical situations [35].

Among the bioengineering applications, sensing devices are becoming increasingly popular. It involves confinement and colloid interaction with a nematic host, and its functioning is based on the amplifying optic effects and small response times. In general, defects of liquid crystals serve as regions of high energy that attract colloids as reported in experiments [26, 36–38] and in simulations [39–44]. Work about defects in anisotropic fluids from topology has been a matter of interest, mainly when the subject of study are colloids immerse in a nematic host [45–49].

The interest on this type of materials lays on finding ways of controlling structures that form within the system, particularly the morphologies found in chiral nematics. Chiral nematics, or cholesterics, were studied from a purely academic perspective since their narrow range of stability ($\sim 1K$) posed significant challenges in technological applications. This type of nematics includes an additional mode of deformation, a continuous inherent rotation of the molecules along an axis. Such rotation causes the emergence of novel morphologies with a network of defects in the bulk of the system. Cholesterics are often studied in cubic confinement and result in what is commonly known as blue phases (BPs), which exhibit lattices of disclination lines with cubic symmetry resembling a simple cubic (SC) structure or a body centered cubic (BCC) structure. Thanks to chemical strategies like doping achiral LCs with chiral components [50–56], enantiomeric mixtures and cross–linking [15, 57], or employing nanoparticles [58], it is possible to observe blue phases over a wider range of temperatures.

Since there is an interplay between the surface events and the bulk, using other geometries that increase the surface to volume ratio is a viable strategy to enhance the response of LC systems, which was achieved by designing nematic phases encapsulated in droplets. LC droplets are used as sensors for antibodies in immunoassays, prescinding from labelling of proteins and complex instrumentation with a sensing range near the nanogram per millimeter scale [59]. Such results, from achiral nematics, marked a precedent and opened a new path for academic research on LCs: designing responsive systems based on droplets phase transitions [34].

The frontier of liquid crystal research is focused on how to stabilize and harness bulk defects for faster, low-energy switching structures. Understanding mechanisms that allow for the manipulation of defect networks require a deep theoretical background and sophisticated simulation methods that allow for the representation of highly non–linear systems. In this work, we aim at studying different simulation tools, as well as compendious studies of confined nematics and strategies to control the final equilibrium states of chiral materials as wells as colloids immersed in nematic hosts.

1.1 Overview

Chapter 2 presents a brief description of the nature of liquid crystals, followed by the definitions of order parameters, and the free energy functional that accounts for the deformation of nematic phases. Afterwards, we present a breif description of different numerical methods employed for interpolating tensorial fields in any domain. First, a meshless interpolation method commonly known as Radial Basis Functions (RBFs) is introduced and some variations that were considered. The other numerical method is Gaussian Quadrature with a Finite Element mesh. The next section presents free energy minimization methods that were employed: a relaxation of the tensor order parameter with the Ginzburg–Landau equation, and a theoretically informed Monte Carlo method presented by Armas-Pérez *et al.* [60, 61].

In chapter 3 we present the results associated with the numerical study of the RBF method in 3D domains with a new methodology to obtain highly accurate estimation of gradients. This

methodology is tested for analytical functions, and then implemented in the relaxation of the free energy functional of a droplet of non-chiral nematic LC.

Chapter 4 contains the results of a comprehensive study of chiral LCs confined in spheroids. From the phase diagrams we are able to explain how morphologies are affected by regions of high curvature, changes in anchoring strength and temperature, as well as some introspective on the nature of chiral systems. Chapter 5 consist on a study of homeotropic and planar particles adsorbed on the surface of a bipolar droplet. In this study we focus on the different assemblies such particles form as well as a broad spectrum of structures of technological interest.

To conclude, chapter 6 contains the final remarks of each aspect presented in previous chapters; in chapter 7 prospective projects are posed in light of the reaches of the theoretically informed Monte Carlo method used in chapter **??**.

1.2 Dissemination of results

The results obtained during this process are being prepared for publication, and are listed as follows:

- "Tactoids of chiral liquid crystals". *V. Palacio–Betancur*, S. Villada–Gil, Y. Zhou, J.C. Armas–Pérez, J.J. de Pablo, J.P. Hernández–Ortiz. **APS March Meeting 2016**. Presented **here.**
- "Educating local radial basis functions using the highest gradient of interest in three dimensional geometries". *V. Palacio–Betancur*, S. Villada–Gil, J.J. de Pablo, and J.P. Hernández–Ortiz. Submitted to **International Journal of Numerical Methods in Engineering.**
- "Hybridization and stability of blue phases via geometrical frustration". *V. Palacio–Betancur*, J.C. Armas–Pérez, S. Villada–Gil, J.P. Hernández–Ortiz, and J.J. de Pablo. To be submitted to **Soft Matter**.
- "Topological dereliction in liquid crystal mediated nano-particle assembly on spherical droplets". J.C. Armas–Pérez, *V. Palacio–Betancur*, J.P. Hernández–Ortiz, and J.J. de Pablo. To be submitted to **Soft Matter**.

- "Liquid crystal phase diagrams from a phenomenological free energy functional description: Landau–de Gennes theory". S. Villada–Gil, *V. Palacio–Betancur*, J.C. Armas–Pérez, J.J. de Pablo, and J.P. Hernández–Ortiz. To be submitted to **Physical Review E**.

Chapter 2
Modeling of Liquid Crystals

The ordering quality of LCs is given by the shape of its molecules, which are classified in three categories: rod-like, disk-like and bent-core. The two first categories are the most common and are often found in biological systems, *e.g.* the lipids in cell membranes are rod-like molecules and the cholesterol is disk-like. A representation of both types is shown in Figure 2.1 with molecules of 5CB (rod-like) and triphenylene (disk-like). The alignment of these molecules is responsible for their optical activity.

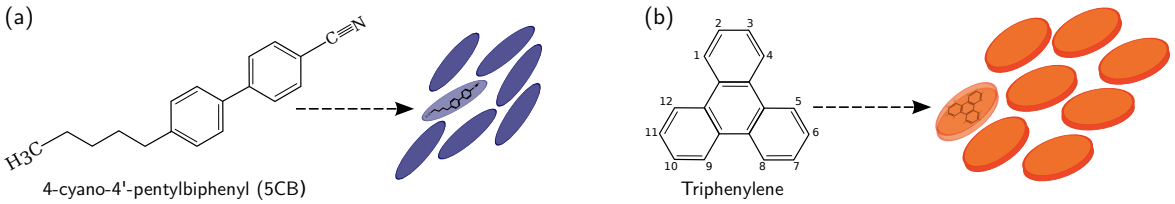

Figure 2.1. Representation of (a) a rod-like molecule of 5CB and (b) disk-like molecule of triphenylene.

Liquid crystals can also be classified as *(i)* thermotropic, *(ii)* lyotropic or *(iii)* metallotropic. Thermotropic liquid crystals are those whose ordering can be altered by heating or cooling of the material. For lyotropic LCs to be observed, it is necessary to reach a critical concentration and it depends on the length and diameter of the molecules. Metallotropic LCs are a mixture of inorganic and organic materials with dependence of temperature. Our main interest is focused on thermotropic liquid crystals, which exist in a specific range of temperature. Any LC system is a collection of distinct mesomorphous phases, or mesophases, each with a specific type of ordering.

The order is defined by the uniformity of the orientation within the domain. In thermotropic LCs the phases range from nematic to smectics as function of the temperature as shown in Figure 2.2.

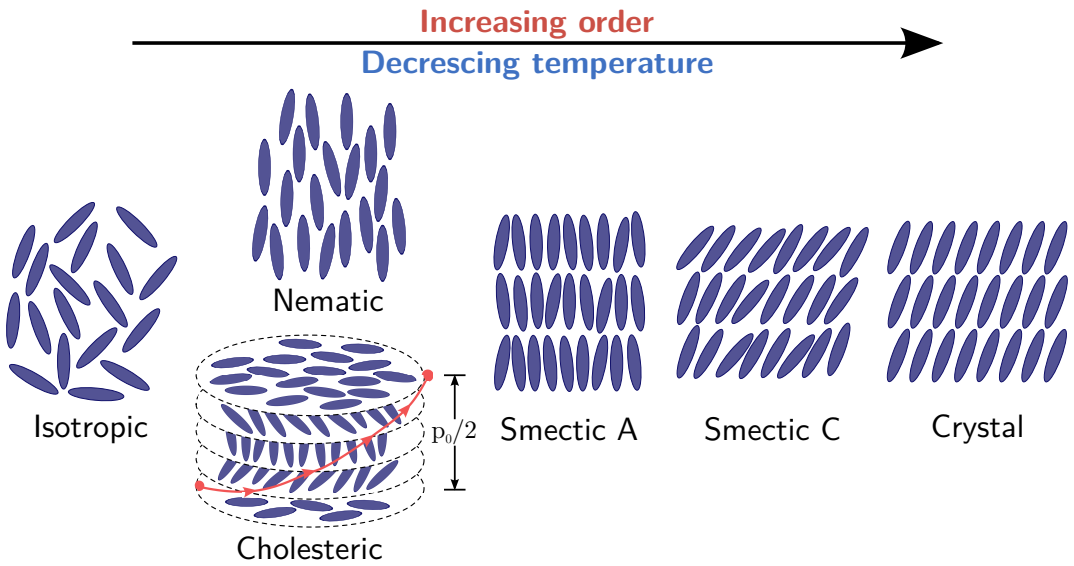

Figure 2.2. Different phases for thermotropic uniaxial liquid crystals as temperature decreases.

After transitioning from the isotropic state we found the nematic phase, which is characterized by long range orientational order along the average molecular orientation, but no positional order. Cholesterics are a special case of nematics in which there is also a supermolecular structure related to a helical rotation of the director, it can be interpreted as nematic layers stacked and the local orientation of each layer rotates respect to the previous one. By decreasing temperature furthermore, we transition to smectic phases, which exhibit positional and orientational molecular order, it is the phase that resembles the most to a crystal before reaching crystallization.

Besides their relationship with temperature, LCs behavior is also influenced by the presence of foreign substances, confinement, or applied external fields. The interaction between the LC molecules and any surface is called anchoring and it dictates the preferred orientation at the surface, the most common ones are homeotropic and planar anchoring.

When molecules realign to match boundary conditions, conflicting directions may arise and the director field becomes singular at some points, thus forming defects. Defects vary in shape, size and location depending on the imposed boundary conditions, geometry and physical properties of

the material. Defects are often characterized by their topological charge, which counts how many times the director rotates around the discontinuity in multiples of π and obeys a conservation law; it is zero in a flat surface and when enclosed in a sphere it must be 2 as required by the Poincaré-Hopf theorem [62].

The frustration, this is the competition between different influences on a physical system, is resolved when there is balance between the elastic energy that penalizes deformations, the interface interaction that promotes a preferred orientation, and the geometry restrictions [63, 64]. For simplicity, the equilibrium configurations of the director field will be called phases.

A comprehensive description of liquid crystalline behavior must be able to capture the variations on the orientation of the molecules in a free domain as well as when confinement or interaction with foreign particles forces a specific orientation. Besides the description of the molecular ordering, free energies penalties exist to determine the most stable configuration of a LC system. This chapter introduces the mathematical tools needed for the modeling of uniaxial nematic liquid crystals. First, we dedicate a section to the definition of different order parameters. Then, the free energy description is presented as the result of three different contributions: bulk, elastic, and surface free energies. A brief description of the formation of topological defects is shown, as well as a general depiction of nematic and cholesteric phases.

2.1 Physics of nematic phases

2.1.1 Order description

The first attempt to quantify the ordering of a LC system consisted of a scalar parameter indicating the degree of isotropy. The definition comes from averaging the molecular orientations and measuring the angle between molecules, θ.

$$S \equiv \frac{1}{2}\langle 3\cos^2\theta - 1\rangle. \tag{2.1}$$

This description is macroscopic and does not capture the minutia in the range of the molecular scale. The next step would be to obtain information of the direction of the molecular alignment $\mathbf{u}$, thus obtaining the director fields $\mathbf{n}$ and $\mathbf{n}'$ where the latter only arises for biaxial molecules. This is depicted in figure 2.3. Recall that for uniaxial molecules, $\mathbf{n}$ is equivalent to $\mathbf{n}'$.

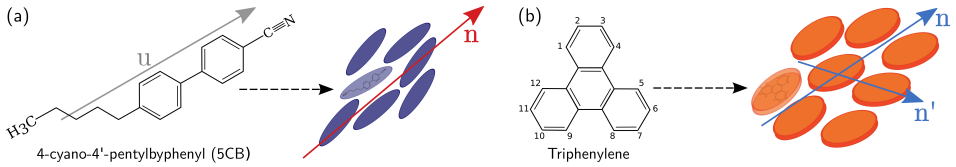

Figure 2.3. Molecular orientation for (a) uniaxial and (b) biaxial molecules. The vector $\mathbf{u}$ indicates the orientation of a single molecule, and $\mathbf{n}, \mathbf{n}'$ are the director vectors.

As mentioned before, the use of liquid crystals is appealing because of the optical particularities that arise from defects. These defects are, by definition, regions where the molecular orientations diverge so any calculations for said region based on vectorial descriptions is not appropriate. To circumvent this issue, the description is taken to the next level with the formulation of a traceless and symmetric tensor, $\mathbf{Q}$. It is defined by the director field and the probability distribution function $\psi_{(\mathbf{n},\mathbf{x},t)}$ of molecular orientations:

$$\mathbf{Q} = \int \mathbf{nn}\psi(\mathbf{n},\mathbf{x},t)\mathrm{d}\mathbf{n} - \frac{\boldsymbol{\delta}}{3}, \tag{2.2}$$

where $\boldsymbol{\delta}$ is the 3×3 identity matrix. Tensor $\mathbf{Q}$ may be written in terms of its eigenvalues in a diagonal form as follows,

$$\mathbf{Q} = \begin{pmatrix} \frac{2}{3}S & & \\ & \eta - \frac{1}{3}S & \\ & & -\eta - \frac{1}{3}S \end{pmatrix} \tag{2.3}$$

According to this representation, tensor $\mathbf{Q}$ can also be written in terms of its eigenvalues [65, 66],

$$\mathbf{Q} = S\left(\mathbf{nn} - \frac{\delta}{3}\right) + \eta\left[\mathbf{n}'\mathbf{n}' - (\mathbf{n}\times\mathbf{n}')(\mathbf{n}\times\mathbf{n}')\right], \tag{2.4}$$

where $S(\mathbf{x})$ is the scalar order parameter, related to the maximum eigenvalue. The biaxiality $\eta(\mathbf{x})$ is related to the other two eigenvalues. The order parameters are bounded by $S \in [-1/2, 1]$,

and $\eta \in [-1/3(1-S), 1/3(1-S)]$. The eigenvectors, $\mathbf{n}$ and $\mathbf{n}'$, define an orthonormal basis $\{\mathbf{n}, \mathbf{n}', (\mathbf{n} \times \mathbf{n}')\}$ for the LC orientation.

This definition of an order parameter allows for a continuous representation of the molecular ordering, and a precise description of regions with defects. The $\mathbf{Q}$ tensor contains all the information for an accurate thermodynamic description of the system, whether the system is in a LC state or during the transitions between these states.

2.1.2 Free energy description

The expressions at static equilibrium that describe this type of material, tipically lead to the Helmholtz free energy taking the form of a polynomial expression in $\mathbf{Q}$ or in S as originally presented by Landau in 1936 [67], and later adapted to liquid crystals by de Gennes in 1969 [3]. Alternatives for the static description include de Maier-Saupe theory [68], and the Onsager theory [69]. For the non-homogeneity of nematic phases, the Oseen theory [70] and later refounded by Frank [71] is very popular since it includes different modes of deformation that carries energetic penalties. More realistic situations include confinement conditions, for which we present different functionals that impose a preferred orientation of the molecules as a boundary condition.

Joining these contributions, the free energy functional is calculated as,

$$F(\mathbf{Q}) = \int \mathrm{d}^3\mathbf{x}\,[f_L(\mathbf{Q}) + f_E(\mathbf{Q}, \nabla\mathbf{Q})] + \oint \mathrm{d}^2\mathbf{x} f_S(\mathbf{Q}) \tag{2.5}$$

where f_L is the Landau–de Gennes free energy, f_E is the elastic free energy, and f_S is the surface free energy. In the following sections each contribution will be explained in more detail.

2.1.2.1 Landau–de Gennes free energy

For the description of the bulk free energy we use a phenomenological approach that serves to characterize the internal structure of the medium. The free energy density is described by a truncated polynomial expansion of the tensor order parameter's invariants [3, 67, 72–74].

$$f_L(\mathbf{Q}) = \frac{1}{2}A(T)\mathrm{tr}(\mathbf{Q}^2) + \frac{1}{3}B\mathrm{tr}(\mathbf{Q}^3) + \frac{1}{4}C\mathrm{tr}(\mathbf{Q}^2)^2,$$

where $A(T), B$, and C are phenomenological coefficients, $\mathrm{tr}\,(\mathbf{M})$ is the trace of the matrix $\mathbf{M}$ and $\mathbf{Q}^2 = Q_{ij}Q_{jk}$. The free energy density in eq. (2.6) predicts a phase transition at a temperature that forces A to vanish. Therefore, it is assumed that A has the form,

$$A(T) = a\,(T - T^*)\,, \tag{2.6}$$

where a is positive and constant, T is the temperature and T^* is a temperature close to the NI transition temperature, T_{NI}.

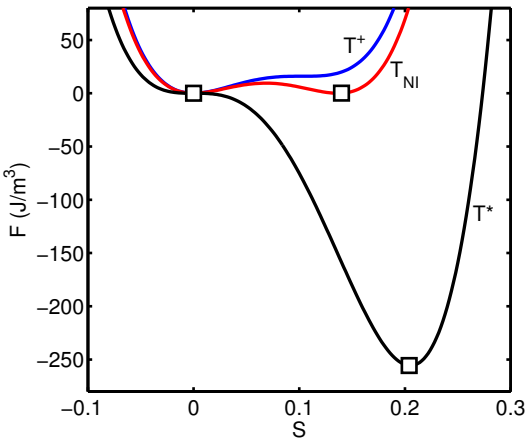

Figure 2.4. Free energy density of the 5CB as a function of the uniaxial order parameter at three different temperatures: T^+, T_{NI}, and T^*. The phenomenological coefficients are: $a = 0.13 \times 10^6 J/m^3K, B = -1.6 \times 10^6 J/m^3, C = 3.9 \times 10^6 J/m^3$, and $T^* = 307.15K$ from [75]. The squares indicate the equilibrium values of the order parameter. This diagram is valid only for $B < 0$.

Through this functional it is possible to study the transition from the isotropic state to the nematic, by differentiating four different temperature regimes. At high temperatures, $T > T^+$, there is a single minimum in the free energy that corresponds to a stable isotropic phase; F has only one minimum at $S = 0$. For $T_{NI} < T < T^+$, the isotropic phase is still the stable state, but there is

an additional local minimum in the free energy at

$$S = -\frac{B}{4C}\left\{1 + \left[1 - 24\frac{aC}{B^2}\left(T - T^*\right)\right]^{1/2}\right\}, \tag{2.7}$$

that corresponds to a metastable nematic phase. On the contrary, for $T^* < T < T_{NI}$ the stable state is the nematic phase, while the isotropic phase is the local free energy minimum. Finally, at $T < T^*$ there is a unique nematic stable phase. At $T = T_{NI}$ the two minima are equivalent, thereby defining the NI transition. Note that this transition shows a discontinuity in the order parameter, ergo it is a first-order transition. This is explained by the odd-order powers of $\mathrm{tr}(\mathbf{Q})$ in the free energy functional.

The form of the free energy density in eq. (2.6) provides additional characteristics and properties for the transitions and phases. For instance, the free energy density is non-linear thus allowing the isotropic phase. The first term drives the NI transition. The inclusion of a third order term causes the NI transition to be first order. It also ensures asymmetry with respect to $\mathbf{Q} \leftrightarrow -\mathbf{Q}$.

From the Doi theory [76], the free energy functional from eq. (2.4) is expressed in terms of another set of phenomenological coefficients. The set consists on A_i coefficients that control the energy scale of the model, and an adimensional parameter U that controls the scalar order parameter S. The free energy functional is rewritten as,

$$f_L(\mathbf{Q}) = \frac{1}{2}A_1\left(1 - \frac{U}{3}\right)\mathrm{tr}(\mathbf{Q}^2) - \frac{1}{3}A_2 U\mathrm{tr}(\mathbf{Q}^3) + \frac{1}{4}A_3 U\mathrm{tr}(\mathbf{Q}^2)^2, \tag{2.8}$$

For a system without boundary restrictions, the order parameter is related to U through the following expression,

$$S_{bulk} = \frac{1}{4} + \frac{3}{4}\sqrt{1 - \frac{8}{3U}} \tag{2.9}$$

To transform the free energy functional from eq. (2.6) to the Doi notation in eq. (2.8) it is necessary to apply the following equivalences,

$$A = A_1 \left(1 - \frac{U}{3}\right) \tag{2.10}$$

$$B = -A_2 U \tag{2.11}$$

$$C = A_3 U \tag{2.12}$$

Following the same analysis for the phase transition lines, values for U analogous to those of T_{NI} and T^+ can be found by assuming a unique value for A_i.

2.1.2.2 Elastic energy: Frank–Oseen theory

The origin of the Frank–Oseen theory lies on an analogy to solid elasticity. When the director field is inhomogeneous, spatial distortions of the molecular orientations caused by the presence of non-zero curvature that later result in a higher free energy. considers that all deformations are a result of three independent modes of variation of $\mathbf{n}$: splay, twist, and bend, using three elastic non-vanishing moduli, k_{11}, k_{22}, and k_{33} as illustrated in figure 2.5.

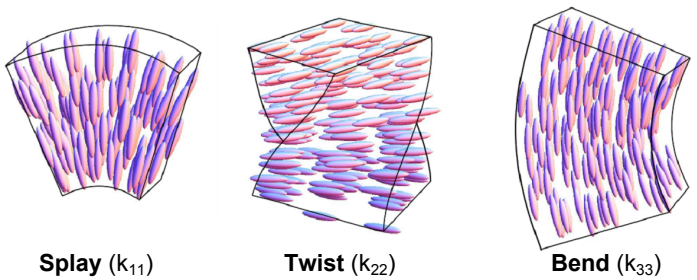

Figure 2.5. Elastic deformation moduli. Figure adapted from [77].

The formulation of this theory in terms of the director field is,

$$f_E = \frac{1}{2}k_{11}\left(\nabla \cdot \mathbf{n}\right)^2 + \frac{1}{2}k_{22}\left(\mathbf{n} \cdot \nabla \times \mathbf{n}\right)^2 + \frac{1}{2}k_{33}|\mathbf{n} \times \left(\nabla \times \mathbf{n}\right)|^2 \tag{2.13}$$

The elastic constants must be positive so the homogeneous state corresponds to a minimum of the elastic free energy. As mentioned before, the use of a phenomenological formulation in terms of vector order parameters is limited to continuous variations of the molecular orientations. The mapping from $\mathbf{n}$ to $\mathbf{Q}$ is only valid for uniaxial molecules and results in the following expression,

$$f_E = \frac{L_1}{2}\frac{\partial Q_{ij}}{\partial x_k}\frac{\partial Q_{ij}}{\partial x_k} + \frac{L_2}{2}\frac{\partial Q_{jk}}{\partial x_k}\frac{\partial Q_{jl}}{\partial x_l} + \frac{L_3}{2}Q_{ij}\frac{\partial Q_{kl}}{\partial x_i}\frac{\partial Q_{kl}}{\partial x_j} \tag{2.14}$$

with the elastic constants L_i related to the elastic moduli by,

$$L_1 = \frac{1}{6S_{bulk}^2}\left(k_{33} - k_{11} + 3k_{22}\right) \tag{2.15}$$

$$L_2 = \frac{1}{S_{bulk}^2}\left(k_{11} - k_{22}\right) \tag{2.16}$$

$$L_3 = \frac{1}{2S_{bulk}^2}\left(k_{33} - k_{11}\right) \tag{2.17}$$

Additional terms might be added to eq. (2.14) in order to describe additional spatial distortions. This is the case for saddle–splay deformations and chirality. Traditionally, the k_{24} constant, corresponding to a saddle-splay deformation, has been neglected because its value is difficult to determine. In curved surfaces or inhomogeneous boundary conditions, the presence of spatial distortion is evident and so, the saddle-splay elastic constant must be included in the free energy [78]. The additional term is:

$$\frac{L_4}{2}\frac{\partial Q_{jk}}{\partial x_l}\frac{\partial Q_{jl}}{\partial x_k}, \tag{2.18}$$

with $L_4 = k_{24}/S_{bulk}^2$ being the elastic constant. The saddle-splay moduli, k_{24}, is bounded by the following two inequalities,

$$-k_{22} \leq k_{24} \leq \min\left(2k_{11} - k_{22}, k_{22}\right) \tag{2.19}$$

The first measurements of the saddle–splay elasticity were done by Ondris–Crawford *et al.* [79] for a confined nematic phase. One of the substantial remarks is that curvature effects add difficulty to determine the value of k_{24}, especially when confinement is in the submicron scale; for supramicron droplets, a stability diagram was obtained for two different configurations of the droplet [80] but

it only provided qualitative appreciations since combined elastic effects (*e.g.* saddle–splay, mixed splay-bend) were neglected due to lack of information.

When treating chiral materials, there is an inherent twist of the director vector of each nematic layer caused by the enantiomeric character of the molecules, as illustrated in figure **??**. The director field follows a helical fashion and completes one revolution in a distance p_0, called the pitch of the material. A material with chirality will not present this type of rotation only if the mixture is racemic. The term that describes this behavior is:

$$\frac{1}{2}L_5\epsilon_{ikl}Q_{ij}\frac{\partial Q_{lj}}{\partial x_k}, \tag{2.20}$$

with ϵ_{ikl} being the Levi–Civita tensor, and L_5 is the elastic constant related to the twist deformation mode k_{22} and the chirality of the system $q_0 = 2\pi/p_0$, by $L_5 = \frac{2}{S_{bulk}^2}q_0k_{22}$. Note that since there is only one gradient that contributes to this type of deformation, the free energy is minimized as the twisting is more frequent.

The one-elastic constant approximation is a common consideration for systems sufficiently large. Due to its simplicity $(k_{11} = k_{22} = k_{33})$, it has been proven appropriate if the geometry has no dramatic changes in curvature [79, 81].

2.1.2.3 Surface free energy

The imposition of a molecular alignement at the surface influences the behavior of the medium so the director takes a compatible orientation that minimizes the free energy, as illustrated in fiugre 2.6. For the homeotropic (perpendicular) anchoring, the second order Rapini–Papoular potential is used [82]:

$$f_S(\mathbf{Q}) = \frac{1}{2}W\left(\mathbf{Q} - \mathbf{Q}^{\mathbf{o}}\right)^2, \tag{2.21}$$

where W represents the anchoring strength and $\mathbf{Q}^{\mathbf{o}}$ is the preferred tensor order parameter at the surface. For degenerate-planar anchoring, the 4th order Fournier–Galatola potential is used [83],

$$f_S(\mathbf{Q}) = \frac{W}{2}\left(\bar{\mathbf{Q}} - \bar{\mathbf{Q}}_\perp\right)^2 + \frac{W}{4}\left(\bar{\mathbf{Q}} : \bar{\mathbf{Q}} - S^2\right)^2, \tag{2.22}$$

where $\bar{Q}_{ij} = Q_{ij} + S\delta_{ij}/3$, $\bar{\mathbf{Q}}_{\perp} = \mathbf{p}\bar{\mathbf{Q}}\mathbf{p}$, $p_{ij} = \delta_{ij} - \nu_i\nu_j$ and ν is the unit vector normal to the surface.

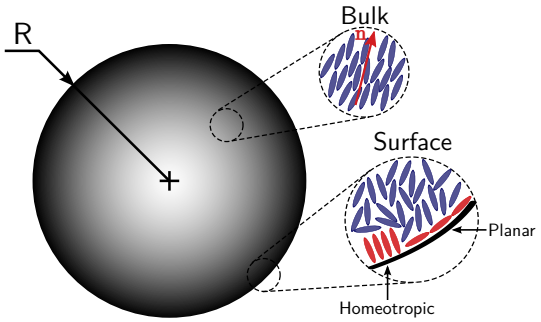

Figure 2.6. Schematic representation of different anchoring conditions for a confined liquid crystal.

2.1.3 Topological defects

When conflicting orientations are present in a LC system, a region where the order is destroyed and the rotational symmetry is broken. That region is called a topological defect, or disclinations, and can also be seen as a singularity of the director field. These defects polarize light [84] and represent regions with higher free energy that is attractive to colloids [52, 85, 86]. It is precisely the ability of LCs to form defects by design, that makes them attractive for technological applications.

Every system that is confined exhibits a competition between the surface orientation and the bulk uniformity, and depending on the anchoring strength it is possible to induce phase transitions [63]. With sufficiently strong anchoring, well defined defects can be differentiated. For achiral LCs, when the anchoring is homeotropic the radial phase is recognized by one defect centered in the bulk where the director field diverges, whether with the tangential anchoring the bipolar phase is observed with two diametrically opposed boojum defects located on the surface. As the anchoring strength decreases, the phases are degenerated and more weakly defined phases are observed, as the twisted radial and the escaped radial (pre-radial) phases. The axial and uniaxial configurations are observed when the anchoring is weak and thus the imposed orientation is easily modified by the elastic forces. These phases are illustrated in figure 2.7.

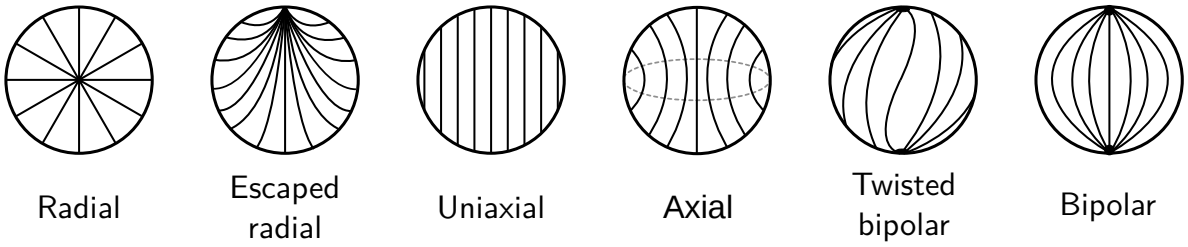

Figure 2.7. Director field configurations for different phases induced by the anchoring conditions in a droplet of nematic liquid crystals.

As chirality is introduced, two regimes define the type of defects. For low chirality, the material is cholesteric and the director field rotates continuously. There are regions with topological charge but not with an abrupt change of the scalar order parameter S. Some of these anormalities are shown in figure 2.8.

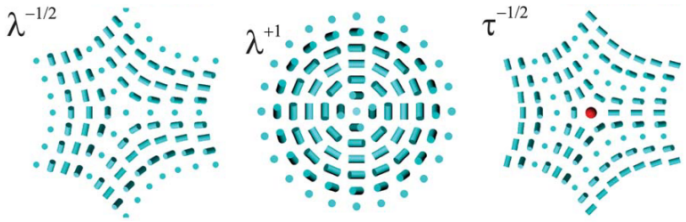

Figure 2.8. Schematic representation of three different cholesteric defects. Adapted from [87].

For materials with high chirality, the director rotates more frequently and regions with double twists join to form defect lines in the bulk, or disclinations. These arrays of defects follow a cubic symmetry of the O^8 type, seen in the body centered cubic structure and called Blue Phase I (BPI), and the O^2 type is called Blue Phase II (BPII) seen in the simple cubic structure. These two phases are illustrated in figure 2.9.

The description of defects will be employed and explained in greater detail in chapter **??**.

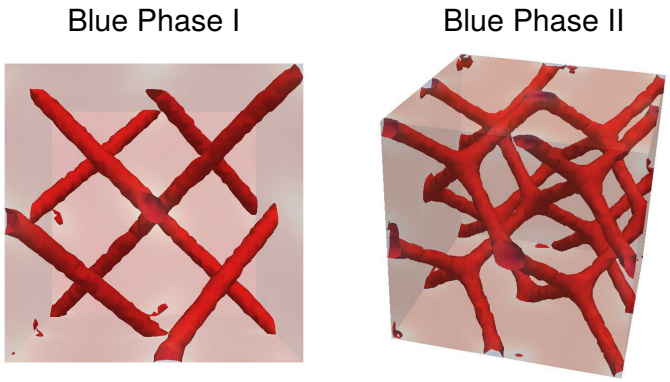

Figure 2.9. Unconstrained symmetric structures of blue phase I (BPI) and blue phase II (BPII).

2.2 Numerical methods

2.2.1 Radial Basis Functions

This method is centred on the linear combination principle. Any set of scattered data can be represented in terms of a set of known functions, called basis functions, as follows:

$$\mathbf{y}(\mathbf{x}) = \sum_{j=1}^{N} \alpha_j \phi(\mathbf{x}_j, \mathbf{x}), \tag{2.23}$$

where the basis functions ϕ depend on the distance between the sample points $\mathbf{x}_j$ and the point of interest $\mathbf{x}$. By solving the linear system $\mathbf{y} = \boldsymbol{\phi} \cdot \boldsymbol{\alpha}$, we capture all the information needed to find data in unknown points. This method was first proposed to interpolate topography data; its simplicity of implementation and versatility makes it the perfect tool for fast calculations. In theory, this method can be applied to problems of n dimensions and can be used to calculate gradients of the known data. However, the limitations of this method are encountered when using large data sets in three dimensions. Alternatives and analysis of this method are presented in more detail in chapter 3.

2.2.2 Gaussian quadrature with Finite Element Method

The integration is done using Gauss-Legendre quadrature over linear and quadratic tetrahedral elements, of the form:

$$I = \int\int\int_T f(x,y,z)\mathrm{d}x\mathrm{d}y\mathrm{d}z \approx \sum_{i=1}^{N} c_m f(x_m, y_m, z_m), \tag{2.24}$$

where T is the tetrahedral element, x, y, z are the coordinates, N is the number of Gauss points or pivotal points, f is the function to be integrated, and c_m are the weights on each point. For the integration we isoparametrize the elements for easier and faster calculation.

The Finite Element-based meshing allows us to capture the nuance of the geometries to perfection and is done using third–party software provided by Argonne National Laboratory [88, 89].

2.3 Free energy minimization

2.3.1 Ginzburg–Landau relaxation

A stable thermodynamic state is obtained for configurations that minimizes the free energy functional $F(\mathbf{Q})$. These minima can be obtained from Ginzburg-Landau isothermal (iso-entropic) relaxation as follows:

$$\frac{\partial \mathbf{Q}}{\partial t} = -\frac{1}{\gamma}\Pi_{\mathbf{Q}}\left(\frac{\delta F}{\delta \mathbf{Q}}\right), \tag{2.25}$$

where γ is a rotational viscosity (or diffusion) coefficient and $\Pi_{\mathbf{Q}}$ is a projector operator that ensures the symmetric and traceless character of $\mathbf{Q}$. The Volterra derivatives are defined by [90]

$$\frac{\delta F}{\delta \mathbf{Q}} = \frac{\partial F}{\partial \mathbf{Q}} - \frac{\partial}{\partial \mathbf{x}} \cdot \frac{\partial F}{\partial \nabla \mathbf{Q}}, \tag{2.26}$$

with proper boundary conditions

$$\frac{\delta F}{\delta \nabla \mathbf{Q}} \cdot \mathbf{v} = 0. \tag{2.27}$$

2.3.2 Theoretically informed Monte Carlo

The free energy functional informs a Monte Carlo relaxation method, as presented in [91, 92]. A Metropolis criteria is followed to sample the $\mathbf{Q}$ tensor. In order to perform a uniform sampling over its 5 independent components, $\mathbf{Q}$ is expressed in terms of an orthonormal tensor basis as presented by Hess *et al.* [93],

$$\mathbf{Q} = \sum_{\nu=1}^{5} a_\nu \left(\mathbf{x}, t\right) \mathbf{T}^\nu \tag{2.28}$$

where the five scalar components a_ν are projections.

The basis are defined by,

$$\begin{aligned}
\mathbf{T}^1 &= \sqrt{3/2}\left[\mathbf{zz}\right]^{ST} = \sqrt{3/2}\left(\delta_{3i}\delta_{3j} - \delta_{ij}/3\right), \\
\mathbf{T}^2 &= \sqrt{2}\left[\mathbf{xy}\right]^{ST} = \sqrt{2}\left(\delta_{1i}\delta_{2j} + \delta_{2i}\delta_{1j}\right)/2, \\
\mathbf{T}^3 &= \sqrt{2}\left[\mathbf{xz}\right]^{ST} = \sqrt{2}\left(\delta_{1i}\delta_{3j} + \delta_{3i}\delta_{1j}\right)/2, \\
\mathbf{T}^4 &= \sqrt{1/2}\left(\mathbf{xx} - \mathbf{yy}\right) = \sqrt{1/2}\left(\delta_{1i}\delta_{1j} - \delta_{2i}\delta_{2j}\right), \\
\mathbf{T}^5 &= \sqrt{2}\left[\mathbf{yz}\right]^{ST} = \sqrt{2}\left(\delta_{2i}\delta_{3j} + \delta_{3i}\delta_{2j}\right)/2.
\end{aligned} \tag{2.29}$$

Here, $[A]^{ST}$ is the symmetric-traceless projection operator, $\mathbf{x}$, $\mathbf{y}$, and $\mathbf{z}$ are the canonical $\Re^3$ basis, and δ_{ij} is the Kronecker delta.

The mapping from Q_{ij} to a_ν is,

$$\begin{aligned}
Q_{11} &= -\frac{a_1}{\sqrt{6}} + \frac{a_4}{\sqrt{2}} \\
Q_{12} &= \frac{a_2}{\sqrt{2}} \\
Q_{13} &= \frac{a_3}{\sqrt{2}} \\
Q_{22} &= -\frac{a_1}{\sqrt{6}} - \frac{a_4}{\sqrt{2}} \\
Q_{23} &= \frac{a_5}{\sqrt{2}}
\end{aligned} \tag{2.30}$$

The sequence of trial moves that are accepted form a Markov chain of configurations, each transition is accepted with probability,

$$P_{acc}\left(o \to n\right) = \min\left[1, \exp\left(-\beta \Delta F\right)\right], \tag{2.31}$$

where $\beta^{-1} = k_B \hat{T}$ with k_B is the Boltzmann constant and $\hat{T}$ is an artificial temperature that is not related to the real temperature of the system; $\Delta F = F\left(\mathbf{Q}_n\right) - F\left(\mathbf{Q}_o\right)$ is the change in the free energy due to an alteration in the old configuration.